

# SIMULTANEOUS SPARSITY-BASED BINARY HYPOTHESIS MODEL FOR REAL HYPERSPECTRAL TARGET DETECTION

Ahmad W. Bitar\*, Loong-Fah Cheong&, Jean-Philippe Ovarlez\*#

\*SONDRA/CentraleSupélec, Plateau du Moulon, 3 rue Joliot-Curie, F-91190 Gif-sur-Yvette, France

&National University of Singapore, Singapore, Singapore

#ONERA, DEMR/TSI, Chemin de la Huniere, 91120 Palaiseau, France

## ABSTRACT

In this paper, a simultaneous sparsity representation-based binary hypothesis (S-SRBBH) model for target detection in hyperspectral image (HSI) is proposed. The S-SRBBH exploits the interpixel correlation within neighboring pixels in HSI, and then, each test pixel is represented by only the background dictionary ( $\mathbf{A}_b$ ) under null hypothesis or from the union of  $\mathbf{A}_b$  and target dictionary ( $\mathbf{A}_t$ ) under alternative hypothesis. Usually, an inner window region (IWR) centered within an outer window region (OWR) contribute in constructing  $\mathbf{A}_b$ . Indeed, the use of IWR has a huge effect on the detection performance since it encloses the targets of interests, but its use requires the information of the size of the targets which is usually hardly available. That is why, this paper also serves to construct  $\mathbf{A}_b$  without IWR by exploiting the low-rank and sparse matrix decomposition (LRaSMD) technique to decompose the HSI into low-rank background HSI and sparse target HSI. Then for each test pixel, a concentric window is located on the low-rank background HSI, and all the pixels (except the center pixel) within the window contribute to form  $\mathbf{A}_b$ . Two real HSIs are used to demonstrate that S-SRBBH achieves good target detection especially when the LRaSMD technique is exploited to construct  $\mathbf{A}_b$ .

## INTRODUCTION TO HYPERSPECTRAL IMAGERY

What is a hyperspectral image (HSI)?:

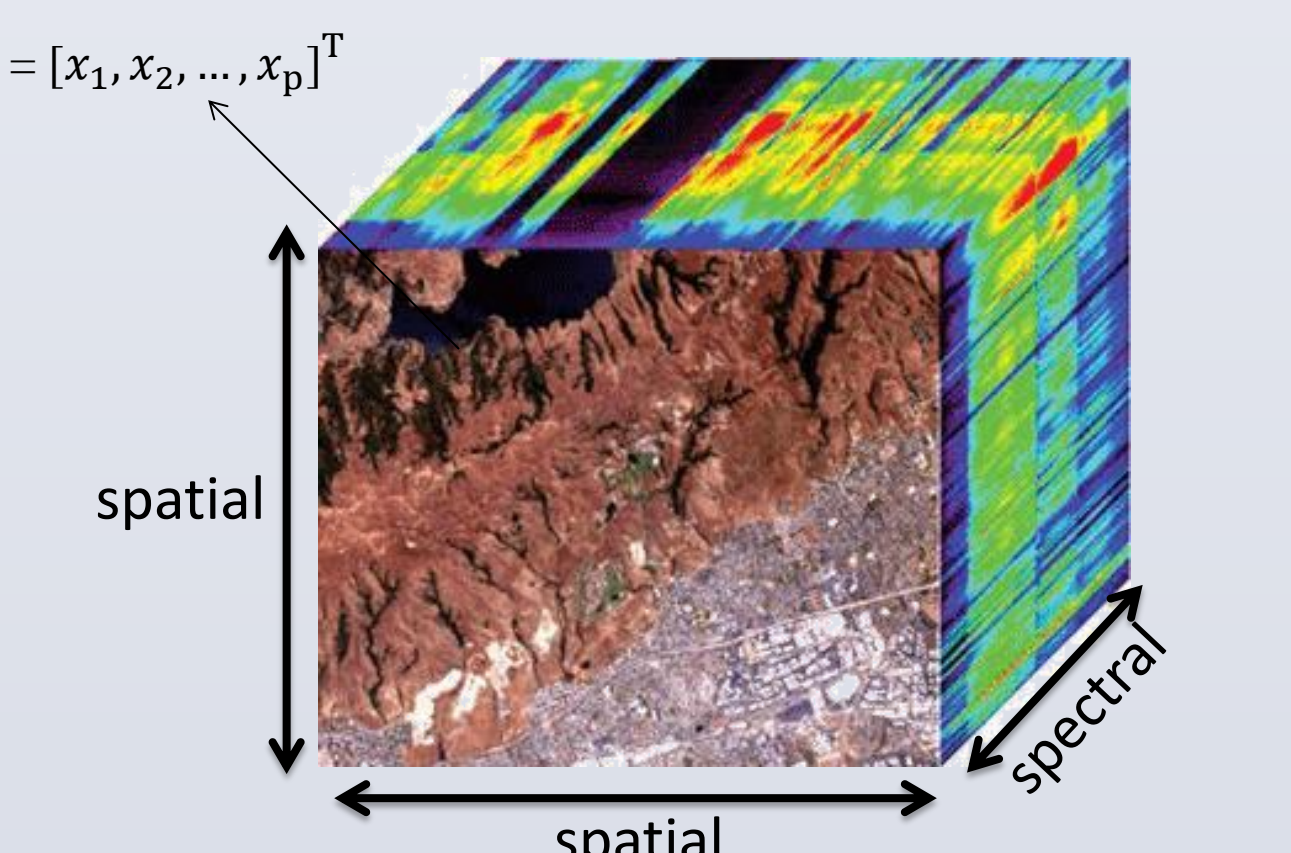


Fig. 1. HSI example

An airborne hyperspectral imaging sensor consists of simultaneously acquiring the same spatial scene in a contiguous and very narrow (10 – 20 nm) spectral wavelength (color) bands [1][2]. The result is thus a 3-D data cube which provides both spatial and spectral information. Thanks to the narrow acquisition, the HSI could have hundreds of thousands of spectral bands.

Each pixel  $\mathbf{x}$  in HSI is represented as a  $p$ -dimensional vector, where  $p$  denotes the total number of spectral bands.

### Hyperspectral Target detection:

With the rich information afforded by the high spectral dimensionality, hyperspectral target detection is not surprisingly one of the most important applications of HSI, where each pixel is labeled as target or background based on its spectral signature [1,2,3,4,5,6,7]. Usually the detection is built using a binary hypothesis testing model:

$$\left\{ \begin{array}{l} H_0: \mathbf{x} = \text{only background (target absent)} \\ H_1: \mathbf{x} = \text{target + background (target present)} \end{array} \right.$$

## MAIN CONTRIBUTIONS (1/2)

Our S-SRBBH model is as follows:

It is expected that for real world HSI, neighboring pixels usually consist of similar materials and thus have similar spectral characteristics [8]. In this case, all the pixels in a small neighborhood can be simultaneously represented as a sparse linear combination of the common training samples but weighted with different coefficients.

We suppose a matrix  $\mathbf{X} = [\mathbf{x}_1, \mathbf{x}_2, \dots, \mathbf{x}_q] \in \mathbb{R}^{p \times q}$ , where  $q$  is the number of pixels in the neighborhood.

• If  $\mathbf{x} \in H_0$ :

$$\begin{aligned} \mathbf{x}_1 &= c_{1,1} \mathbf{a}_1^b + c_{1,2} \mathbf{a}_2^b + \dots + c_{1,N_b} \mathbf{a}_{N_b}^b \\ &\quad \vdots \\ \mathbf{x}_q &= c_{q,1} \mathbf{a}_1^b + c_{q,2} \mathbf{a}_2^b + \dots + c_{q,N_b} \mathbf{a}_{N_b}^b \end{aligned}$$

$$\mathbf{X} = [\mathbf{a}_1^b, \mathbf{a}_2^b, \dots, \mathbf{a}_{N_b}^b] [\mathbf{c}_1, \mathbf{c}_2, \dots, \mathbf{c}_q] = \mathbf{A}_b \mathbf{C}_b \quad (1)$$

where  $\mathbf{a}_1^b, \mathbf{a}_2^b, \dots, \mathbf{a}_{N_b}^b$  are the background training samples,  $N_b$  is the total number of background training samples,  $\mathbf{A}_b \in \mathbb{R}^{p \times N_b}$ ,  $\mathbf{C}_b \in \mathbb{R}^{N_b \times q}$ .

• If  $\mathbf{x} \in H_1$ :

$$\begin{aligned} \mathbf{x}_1 &= c'_{1,1} \mathbf{a}_1^b + c'_{1,2} \mathbf{a}_2^b + \dots + c'_{1,N_b} \mathbf{a}_{N_b}^b \\ &\quad + z_{1,1} \mathbf{a}_1^t + z_{1,2} \mathbf{a}_2^t + \dots + z_{1,N_t} \mathbf{a}_{N_t}^t \\ &\quad \vdots \\ \mathbf{x}_q &= c'_{q,1} \mathbf{a}_1^b + c'_{q,2} \mathbf{a}_2^b + \dots + c'_{q,N_b} \mathbf{a}_{N_b}^b \\ &\quad + z_{q,1} \mathbf{a}_1^t + z_{q,2} \mathbf{a}_2^t + \dots + z_{q,N_t} \mathbf{a}_{N_t}^t \end{aligned}$$

$$\begin{aligned} \mathbf{X} &= [\mathbf{a}_1^b, \mathbf{a}_2^b, \dots, \mathbf{a}_{N_b}^b] [\mathbf{c}'_1, \mathbf{c}'_2, \dots, \mathbf{c}'_q] \\ &\quad + [\mathbf{a}_1^t, \mathbf{a}_2^t, \dots, \mathbf{a}_{N_t}^t] [\mathbf{z}_1, \mathbf{z}_2, \dots, \mathbf{z}_q] \\ &= [\mathbf{A}_b \mathbf{A}_t] (\mathbf{z}_t) = \mathbf{A} \mathbf{S}. \end{aligned} \quad (2)$$

where  $\mathbf{a}_1^t, \mathbf{a}_2^t, \dots, \mathbf{a}_{N_t}^t$  are the target training samples,  $N_t$  is the total number of target training samples,  $\mathbf{A}_t \in \mathbb{R}^{p \times N_t}$ ,  $\mathbf{C}'_t \in \mathbb{R}^{N_t \times q}$ ,  $\mathbf{Z}_t \in \mathbb{R}^{N_t \times q}$ ,  $\mathbf{A} \in \mathbb{R}^{p \times (N_b+N_t)}$ , and  $\mathbf{S} \in \mathbb{R}^{(N_b+N_t) \times q}$ .

Both  $\mathbf{C}_b$  and  $\mathbf{S}$  stand to be sparse in rows:

$$\hat{\mathbf{C}}_b = \operatorname{argmin}_{\mathbf{C}_b} \|\mathbf{X} - \mathbf{A}_b \mathbf{C}_b\|_F \text{ s.t. } \|\mathbf{C}_b\|_{0,2} \leq K_0 \quad (3a)$$

$$\hat{\mathbf{S}} = \operatorname{argmin}_{\mathbf{S}} \|\mathbf{X} - \mathbf{A} \mathbf{S}\|_F \text{ s.t. } \|\mathbf{S}\|_{0,2} \leq K'_0 \quad (3b)$$

where  $K_0$  and  $K'_0$  denote the upper bound on the sparsity level (we assume  $K_0 = K'_0$ ) and  $\|\cdot\|_{0,2}$  is the  $L_{0,2}$ -norm that counts the number of non-zero rows in the matrix.

## MAIN CONTRIBUTIONS (2/2)

Sub-problems (3a) and (3b) are non-convex and NP-HARD  $\Rightarrow$  we solve them using the Simultaneous Orthogonal Matching Pursuit (SOMP) greedy algorithm [9].

We obtain our detector:

$$D_{S-SRBBH}(\mathbf{x}) = \|\mathbf{X} - \mathbf{A}_b \hat{\mathbf{C}}_b\|_F - \|\mathbf{X} - \mathbf{A} \hat{\mathbf{S}}\|_F \stackrel{\frac{H_1}{H_0}}{>} \gamma \quad (4)$$

where  $\gamma$  is a prescribed threshold value.

### Construction of the background and target dictionaries:

#### $\mathbf{A}_t$ construction:

There can be a priori information about the target of interest to be detected. Therefore, the  $\mathbf{A}_t$  is known and can be constructed using the MORTAN atmospheric modeling program [10] to generate a large number of target signatures under various atmospheric conditions. In addition, the  $\mathbf{A}_t$  can also be formed by the USGS [11] and the ASTER [12] digital spectral libraries.

In our work, we construct it from some of the target pixels present in the global image scene.

#### $\mathbf{A}_b$ construction:

1. The targets in HSI always occupy a small part of the entire image and thus are characterized by the sparsity property (in the spatial domain) [13][14].
2. The background is usually assumed to have a low rank property [13][14].

Based on the aforementioned analysis, the Low rank and Sparse Matrix Decomposition (LRaSMD) technique [15][16] is exploited to construct  $\mathbf{A}_b$

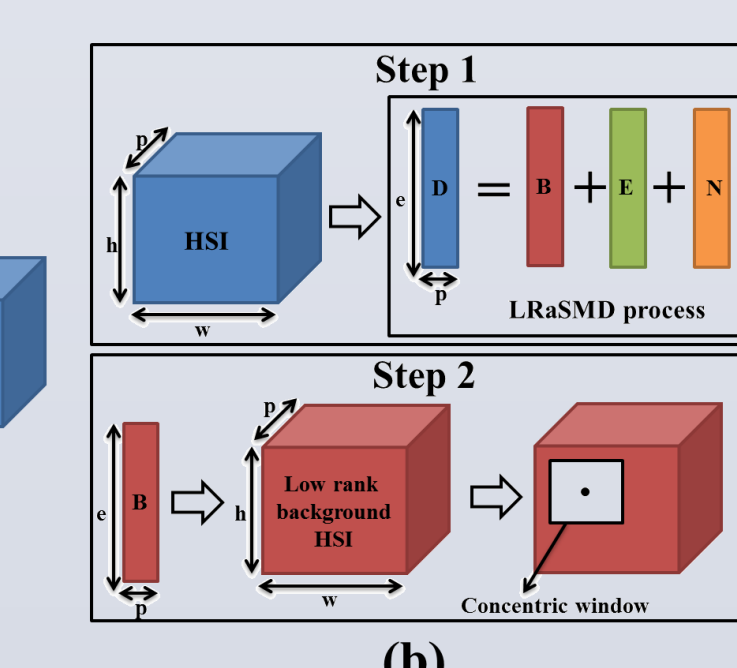


Fig. 2.  $\mathbf{A}_b$  construction: (a) Traditional method (b) via the LRaSMD technique

For any HSI of size  $h \times w \times p$ , where  $h$  and  $w$  are the height and width of the image scene, respectively, and after rearranging it into a two-dimensional matrix  $\mathbf{D} \in \mathbb{R}^{h \times p}$ , where  $e = h \times w$ , the model of HSI can be modeled as  $\mathbf{D} = \mathbf{B} + \mathbf{E} + \mathbf{N}$ , where  $\mathbf{B}$  is the (low-rank) background matrix,  $\mathbf{E}$  is the (sparse) target matrix, and  $\mathbf{N}$  is usually assumed to be independent and identically distributed Gaussian noise.

After that the background matrix  $\mathbf{B}$  and the target matrix  $\mathbf{E}$  are being estimated using the SSGoDec optimization algorithm [17], we use only the estimation of  $\mathbf{B}$  and we resize it to a cube of the same size  $h \times w \times p$  (we shall call it as low-rank background HSI). Next, for each test pixel, we create a concentric window (on the low-rank background HSI), and all the pixels (except the center pixel) within the window will each contribute to one column in  $\mathbf{A}_b$ .

## RESULTS

The first HSI (DATA)[18] is a 201×200 image and consists of 167 spectral bands. We have only used a small zone (pixels in rows 1 to 150 and columns 80 to 180) for the detection. The main background materials of the selected zone are road and vegetation. There are three cars on the road and we will consider them as targets to be detected. Figure 3 exhibits the mean power in dB over the 167 bands.

The second HSI is the Pavia Center City (PaviaC) [14]. It is a 1096 × 1096 image and consists of 102 bands in wavelengths ranging from 430 to 860 nm. We used a small zone (pixels in rows 1 to 130 and columns 223 to 350) for the detection. The main background materials of this zone are bridge and water. There are some vehicles on the bridge and bare soil near the bridge pier and hence they will be selected as targets to be detected. Figure 8 exhibits the mean power in dB over the 102 bands.

- Case 1: using Figure 2(a) with IWR of size 5 × 5,
- Case 2: using Figure 2(a) but without IWR (and by excluding the test pixel),
- Case 3: using Figure 2(b).

We evaluate the target detection performance of S-SRBBH by comparing it to some others (AMF [19][20], ANMF [21], MSD [22] and SRBBH [23]) on the three cases.

Note that if  $q = 1$ , we return back to the SRBBH model. Hence, the S-SRBBH can be considered as a generalization of SRBBH when  $q > 1$ .

The detection performances are evaluated quantitatively by the receiver operating characteristics (ROC) curves [14][23] which describe the probability of detection ( $P_d$ ) as a function of probability of false alarm ( $P_{fa}$ ).

In Case 1, the OWR is of size 15 × 15  $\Rightarrow N_b = 200 \Rightarrow \mathbf{A}_b \in \mathbb{R}^{p \times 200}$ .

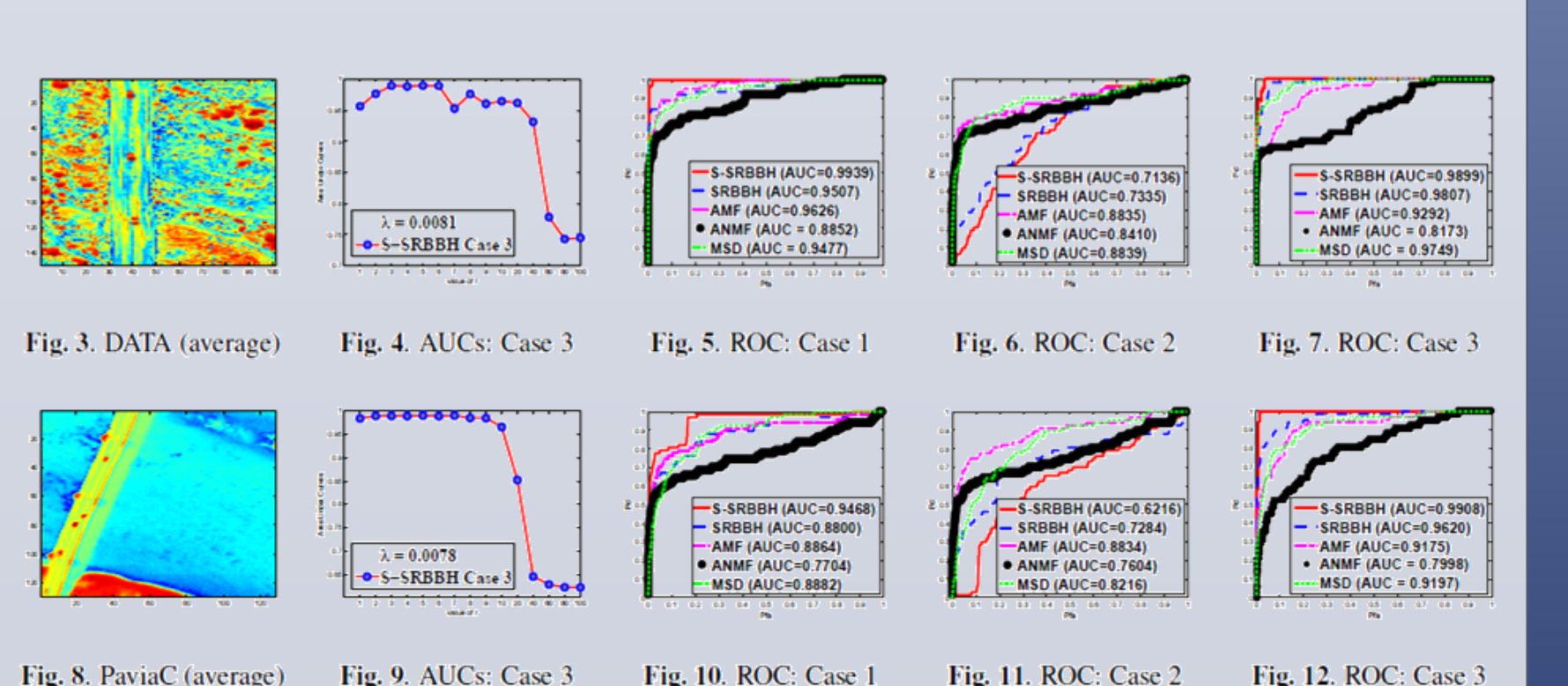
In both Case 2 and 3, the concentric window is of size 15 × 15  $\Rightarrow N_b = 224 \Rightarrow \mathbf{A}_b \in \mathbb{R}^{p \times 224}$ .

We select  $N_t = 9 \Rightarrow \mathbf{A}_t \in \mathbb{R}^{p \times 9}$ .

We set  $K_0 = K'_0 = 8$ . We choose  $q = 25$ , that is, a neighborhood of size 5 × 5. Importantly, the same Case (Case 1, 2 or 3) applied to construct  $\mathbf{A}_b$  for S-SRBBH is also applied to all the other detectors in comparison.

The covariance matrix in AMF, ANMF is estimated via the Fixed Point (FP) estimator [24] and then shrunk towards the identity matrix [25].

In the case of MSD, the eigenvectors corresponding to the significant eigenvalues of the FP matrices obtained from  $\mathbf{A}_t$  and  $\mathbf{A}_b$  are used to generate the basis for target and background subspaces, respectively [26].



## CONCLUSION

In this paper, we first developed the S-SRBBH model that is similar to SRBBH but it further considers the interpixel correlation in hyperspectral imagery. Then, we served to achieve good target detection even without using an IWR in the  $\mathbf{A}_b$  construction. This is done by first, exploiting the LRaSMD technique based on the SSGoDec optimization algorithm to approximately separate the given HSI into low-rank background HSI and sparse target HSI. Second, for each test pixel, a concentric window is used on the low-rank background HSI and the pixels (except the center pixel) within the window are used to form  $\mathbf{A}_b$ . Two real hyperspectral images demonstrate that S-SRBBH has higher AUC values than all of the other detectors in comparison for both Case 1 and Case 3. In addition, exploiting the LRaSMD to construct  $\mathbf{A}_b$  for both S-SRBBH and SRBBH greatly improves their target detection performances as shown between Case 2 and Case 3.

## REFERENCES

- [1] G. Shaw and D. Manolakis, "Signal processing for hyperspectral image exploitation," IEEE Signal Processing Magazine, vol. 19, no. 1, pp. 12–16, Jan 2002.
- [2] D. Manolakis, D. Marden, and G. Shaw, "Hyperspectral image processing for automatic target detection applications," Lincoln Laboratory Journal, vol. 14, no. 1, pp. 79–116, 2003.
- [3] D. Manolakis, E. Truslow, M. Pieper, T. Cooley, and M. Brueggeman, "Detection algorithms in hyperspectral imaging systems: An overview of practical algorithms," IEEE Signal Processing Magazine, vol. 31, no. 1, pp. 24–33, Jan 2014.
- [4] D. Manolakis, R. Lockwood, T. Cooley, and J. Jacobson, "Is there a best hyperspectral detection algorithm?" Proc. SPIE 7334, p. 733402, 2009.
- [5] D. Manolakis and G. Shaw, "Detection algorithms for hyperspectral imaging applications," Signal Processing Magazine, vol. 19, no. 1, pp. 29–43, 2002.
- [6] J. Frontera-Pons, F. Pascal, and J. P. Ovarlez, "False-alarm regulation for target detection in hyperspectral imaging," in Computational Advances in Multi-Sensor Adaptive Processing (CAMSAP), 2013 IEEE 5th International Workshop on, Dec 2013, pp. 161–164.
- [7] J. Frontera-Pons, M. A. Vaganzas, S. Velasco-Forero, F. Pascal, J. P. Ovarlez, and J. Chanussot, "Robust anomaly detection in hyperspectral imaging," in 2014 IEEE Geoscience and Remote Sensing Symposium, July 2014, pp. 4604–4607.
- [8] Y. Chen, N. M. Nasrabadi, and T. D. Tran, "Simultaneous joint sparsity model for target detection in hyperspectral imagery," IEEE Geoscience and Remote Sensing Letters, vol. 8, no. 4, pp. 676–680, July 2011.
- [9] J. A. Tropp, A. C. Gilbert, and M. J. Strauss Martin, "Algorithms for simultaneous sparse approximation: Part I: Greedy pursuit," Signal Process., vol. 86, no. 3, pp. 572–588, Mar. 2006.
- [10] A. Berk, L. Bernstein, and D. Robertson, "MORTAN: A moderate resolution model for LOWTRAN 7," Tech. Rep. GLTR-90-0122, Geophysics Laboratory, Bedford, MA, 1989.
- [11] Roger N. Clark, Gregg A. Swazey, Andrea J. Gallagher, Trude V.V. King, and Wendy M. Calvin, "The U.S. Geological Survey Digital Spectral Library: Version 1: 0.2 to 3.0 microns," Open file report, U.S. Geological Survey, 1993.
- [12] A.M. Baldrige, S.J. Hook, C.I. Grove, and G. Rivera, "The ASTER Spectral Library Version 2.0," Remote Sensing of Environment, vol. 113, pp. 711–715, 2009.
- [13] Shih-Yu Chen, Shiming Yang, Konstantinos Kalpakis, and Chein-I Chang, "Low-rank decomposition-based anomaly detection,"